Journal of Applied Polymer Science

Flexible shielding layers for solar cells in space applications

J. Feenstra,[1] R. H. van Leest,[1] N. J. Smeenk,[1] G. Oomen,[2] E. Bongers,[2] P. Mulder,[1] E. Vlieg,[1] J. J. Schermer[1]

[1]Institute for Molecules and Materials, Radboud University, Heyendaalseweg 135, AJ Nijmegen 6525, The Netherlands
[2]Airbus Defense and Space Netherlands, Mendelweg 30, CS Leiden 2333, The Netherlands
Correspondence to: J. Feenstra (E-mail: j.feenstra@science.ru.nl)

ABSTRACT: The development of flexible, thin-film, and high-efficiency III–V solar cells enables the design of new flexible, lightweight solar arrays for space applications. A requirement for these solar panels is the replacement of the rigid coverglasses by a flexible shielding layer. In this work, three candidate materials based on commercially available polyimides and synthesized polysiloxanes for such a shielding layer are compared with respect to their ease of synthesis, transparency. Polysiloxanes based on methyltrimethoxysilane (MTMS) based siloxane (MBS) showed the best reproducibility in synthesis of layers of the required thickness of about 300 μm with sufficient transparency and was therefore selected for further analysis. It was demonstrated that the MBS material could be doped with Ce to increase the radiation hardness. Showing virtually no loss of volatile condensable components in outgassing tests it can be concluded that the properties MBS are found suitable for further space qualification testing. © 2016 Wiley Periodicals, Inc. J. Appl. Polym. Sci. **2016**, *133*, 43661.

KEYWORDS: degradation; functionalization of polymers; inorganic polymers; mechanical properties; optical and photovoltaic applications photovoltaics; polyimides; polysiloxane; shielding layers; space applications; TEOS

Received 10 September 2015; accepted 22 March 2016
DOI: 10.1002/app.43661

INTRODUCTION

In recent years, the epitaxial lift-off (ELO) technique is increasingly recognized as a method to reduce the costs of III–V solar cells for space applications and concentrator systems.[1–3] ELO separates single crystalline thin-film structures from their growth template (GaAs, Ge, or InP wafer) by selective etching of an intermediate release layer.[4–8] Cost reduction is achieved by reusing the expensive wafers for the production of subsequent thin-film solar cell structures.[9] It was demonstrated that the use of the ELO technique can result in flexible, thin-film solar cells, with efficiencies equal to that of cells on their growth substrate.[10] An example of a flexible thin-film solar cell is shown in Figure 1. As a result of photon confinement,[11,12] single-junction thin-film structures with efficiencies that surpass the best performance of wafer-based cells were reported.[13–15] Furthermore, the ELO technique is beneficial for an inverted metamorphic triple-junction solar cell,[16] where substrate removal is required for the cell to operate.

Most of the III–V solar cells produced nowadays are used for powering satellites. For this application, the current generation wafer-based III–V cells are mounted on rigid carbon fiber/aluminum honeycomb panels for stability and covered with glass shielding to protect the cells from the harsh environment encountered in space [see Figure 2(a)]. The coverglass typically has a thickness of 100 μm and contains approximately 2% cerium,[17] because this element absorbs the high-energy UV photons encountered in space, thereby protecting underlying layers (adhesive and solar cell). At the same time, cerium prevents damage to the borosilicate glass into which it is incorporated. As described in more detail by Treadaway *et al.*,[18] radiation damage in glass produces displaced, trapped electrons, and positive holes due to electron displacement. This gives rise to absorption bands, since the trapped electrons form color centers ultimately leading to reduced transmission in the glass. The damage is prevented by Ce(IV) ions absorbing the displaced electrons, while Ce(III) ions eliminate the holes by electron donation.[18–20]

For space applications, the weight of the solar panel should be as low as possible. The use of thin-film ELO cells on a metal foil carrier, as shown in Figure 2, would immediately reduce panel weight with more than 25%. In addition, a much larger weight reduction is possible on panel level since a flexible thin-film solar cell does not require a rigid support, which is currently applied. However, the current rigid panel mount is not solely applied for the support of the brittle wafer-based solar cell but additionally provides support for the cerium doped coverglass (CMX). In order to facilitate the use of a lightweight

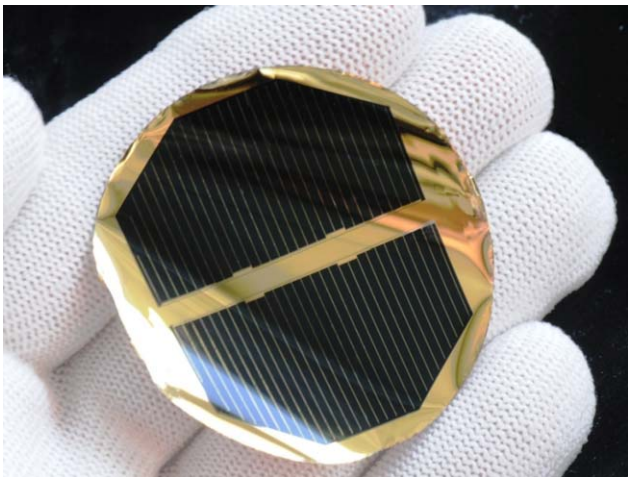

Figure 1. Flexible thin-film solar cells on a thin metal foil produced using the ELO technique. [Color figure can be viewed in the online issue, which is available at wileyonlinelibrary.com.]

solar cell combined with a flexible lightweight mount, also a flexible replacement for the rigid coverglass is required. Aiming for an equal protection at the front and the backside of the thin-film cell, Figure 2(c) shows that an ultimate weight reduction of more than 75% can be obtained compared to the currently applied space solar panels. However, the first goal aimed for is to replace the currently applied aluminum honeycomb/Carbon Fiber Reinforced Plastic (CFRP) sandwich with a thickness of 22 mm by a flat single CFRP plate of about 0.5 mm. Besides weight reduction, this would provide an enormous reduction in volume required to stow the solar modules during launch while deployment of this structure can take place in a similar way as the current rigid panels. Without the support of the Al honeycomb structure, the stability of the CFRP will be insufficient for the CMX coverglass but more than sufficient for most polymer based layers, as the protection layer during deployment will only be subjected to very moderate bending.

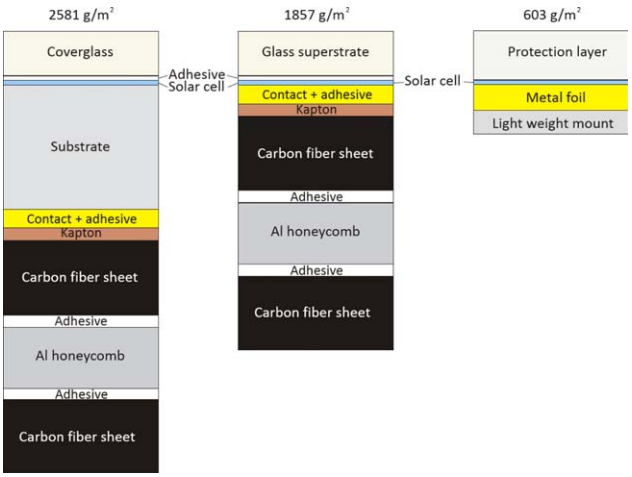

Figure 2. Mass distribution for different solar panel configurations: (a) current solar panel configuration, (b) configuration with the wafer removed, and (c) the flexible panel configuration. The dimensions of the components are depicted proportional to their mass, not to their actual thickness. [Color figure can be viewed in the online issue, which is available at wileyonlinelibrary.com.]

For a flexible and transparent shielding layer the use of polymers is the obvious choice. However, most polymers are not able to withstand the harsh space environment. In particular, high-energy UV radiation and atomic oxygen (ATOX) are expected to be damaging to polymers. UV photons cause radical formation, leading to material loss and the formation of chromophores, and thus giving unwanted darkening of the polymer material.[21] Atomic oxygen (ATOX), which is present in low earth orbits, is also very efficient in breaking organic bonds, resulting in erosion of the polymer structures that are supposed to protect the cell from irradiation by charged particles.[22] In addition, the high vacuum of space is known to cause outgassing of volatile components which can condense and thereby contaminate other parts of the spacecraft. Therefore, it is essential to perform outgassing experiments to test material stability under vacuum conditions prior to their application in space related products.

In this study, we provide a first step towards transparent flexible shielding layers for thin-film solar cells in space applications by selection, synthesis, and examination of several candidate materials. Based on the above described requirements and material properties reported in literature, several materials were selected and tested for their possible suitability as a transparent flexible shielding using the currently applied CMX glass as a benchmark. Shielding is largely determined by the mass encountered by the irradiated particles, therefore, the product of layer thickness and material density is a measure for the shielding capacity. As the density of CMX glass (2.6 g/cm^3) is typically 2–3 times higher than that of the polymer layers to be evaluated, these polymer layers should be 2–3 times thicker than the typical CMX cover to obtain at least equal shielding capacity. For this reason, the aim of this study is to synthesize 300 μm thick layers. In this study, we evaluate the ease of reproducible synthesis and application of the layers as a coating on a substrate and the transparency of the material in the 300–1250 nm wavelength range to assure optimal performance in combination with a triple junction Inverted Meta Morphic (IMM) cell. Only the best performing material on these criteria is used to further evaluate the possibility to dope the layers with Ce, which is known to increase shielding for CMX glass, and the stability of the materials under vacuum. The stability of the materials under vacuum conditions should be such that it can be space qualified, i.e., less than 0.1% weight loss by outgassing of volatile condensable components. These vacuum tests took place at the facilities at European Space Research and Technology Centre (ESTEC).

MATERIAL SELECTION

Three types of materials have been selected, one type of polyimide and two types of polysiloxane, based on prior knowledge or theoretical considerations concerning the bond strengths which should be able to withstand the conditions encountered in space.

Polyimides

Polyimides are one of the few types of organic material that have proven to be UV-resistant[23,24] and were therefore chosen as a starting material for this study. It is known that ATOX induces mass loss by eroding the polyimide and degrades its transparency.[25,26] Therefore, a silica or silicone component needs to be added, which in an ATOX environment forms a passivating silica layer when the polyimide at the surface has been eroded. This silica layer should protect the underlying polyimide from further erosion by ATOX. Recently, such hybrid materials of polyimides and silica components have attracted much attention for the use in space applications, mainly for use on external spacecraft surfaces (e.g., thermal insulation blankets).[27] For these applications flexible layers are desired, but they are not necessarily transparent (most polyimides are yellow or brown in color). In this study, we will evaluate the syntheses and applicability of an optically clear polyimide, in which small (<2 nm) polyhedral oligomeric silsesquioxanes (POSS) particles are embedded.[27]

Polysiloxanes

Another class of flexible shielding materials to be considered are polysiloxanes (e.g., silicones). Several space qualified silicone adhesives are commercially available. These are typically used to adhere the currently applied cerium doped coverglasses on top of solar cells. Silicones have the advantage that they form a passivating silica layer in an ATOX environment, preventing further erosion.[28] This means no additions to a polysiloxane material are needed to make it ATOX resistant. However, they are known to darken when directly (i.e., without a coverglass) exposed to UV light. Also, the mechanical properties change after UV exposure, indicating that polymer degradation occurs most likely in the form of bond breaking which results in a reduction of the average chain length or a reduction in the crosslink density.[29] SiO_2 (silica or quartz) does not show visible degradation upon UV irradiation, indicating that the degradation is mainly caused by the organic groups in the silicones. This is confirmed by the work of Zimmermann,[30] who showed that silicones with larger organic groups, for example phenyl groups, degrade faster. Most commercially available silicones are cured in a platinum-catalyzed hydrosilylation reaction. This results in materials with both Si–O and Si–C–C–Si bonds in the polymer backbone and a Pt-catalyst in the final material. UV photons have sufficient energy to induce cleavage of the C–C or Si–C bonds, leading to decreasing polymer chain lengths, thereby changing material properties.[29] In this process, chromophore species can be formed in the material, leading to the discoloration (darkening) of the silicone.

To avoid the presence of organic moieties (i.e., Si–C, C–C and C–H bonds) in the polymer backbone of polysiloxanes, we have applied a sol–gel reaction for the synthesis of polysiloxanes. This synthesis procedure should result in a polymer that has a backbone that consists only of Si–O–Si groups, so that upon UV exposure the polymer chain length does not decrease. This material still contains methyl groups, which is unavoidable if a flexible material is desired (without the methyl groups amorphous silica is formed). However, these organic groups are only present as side-groups, not in the polymer backbone and the number of them is minimized. Two types of polysiloxane-based materials are studied for their possibilities to be applied as a shielding layer. The first type is a silica-silicone hybrid based on tetraethoxysilane (TEOS), which is a known silica component for transparent hybrid organic/inorganic networks,[31] combined with polydimethoxysilane (PDMS). The synthesis of this TEOS-PDMS combination was previously demonstrated by Mackenzie *et al.*[32] The second polysiloxane type material to be studied involves a methyltrimethoxysilane (MTMS) based siloxane (MBS) and is chosen because their flexibility was reported to be tunable depending on the type and concentration of non-reactive side-group components.[33,34]

EXPERIMENTAL

The goal of this work is to create a shielding layer that can be cast directly on top of a solar cell in a single step procedure. While in practice the shielding layer will always be on a carrier (e.g., the solar cell), it is more convenient for the characterization of the synthesized materials to use freestanding films. Therefore, where possible, freestanding films were synthesized in this work. Since the stopping power of the shielding layer depends mainly on the thickness and density of the material, ergo the mass encountered by the radiation, for each material proposed here, a density study determines the desired thickness of the films. Thereby, protective possibilities should be at least similar to those of the currently used CMX coverglass in the rigid panel configuration.

Synthesis and Application

POSS Films. The polyimide-POSS was obtained in powder form from a commercial supplier (Corin XLS from ManTech). After dissolving it in methyl isobutyl ketone (typically 1:4 w/w of polyimide to solvent), it was casted or spin coated onto a substrate to produce films of varying thicknesses. A single spin coating step (1000 rpm) resulted in layers of 5–10 μm. Successive spin coating runs were applied to obtain films with thicknesses up to 30 μm. To achieve thicker layers, multiple casting steps were applied (each casting step added approximately 25 μm) to obtain films with a final thickness of 50–200 μm (density analysis indicated that about 170 μm polyimide-POSS layer thickness is required to obtain a similar shielding level as 100 μm CMX coverglass). The films were kept in a clean room environment during spin coating/casting and intermediate drying steps to minimize contamination of the surface before a new layer was casted on top. The adhesion of the films to the substrate on which they were produced was such that they could not be removed. Therefore, plastic substrates (cellulose acetate) were used to produce flexible samples while glass slides were used as substrates to facilitate measurements of spectrally resolved transmission.

TEOS-PDMS Films

For the synthesis of the silica–silicone hybrid material, tetraethoxysilane (TEOS) and hydroxyl-terminated polydimethylsiloxane (PDMS, average weight 550 g/mol) were mixed, in various ratios ranging from 2:1 to 1:2, in a mixture of iso-propanol (IPA) and tetrahydro furan (THF) in ratios ranging from respectively 1:1 to 1:2.[35] THF prevents phase separation of the

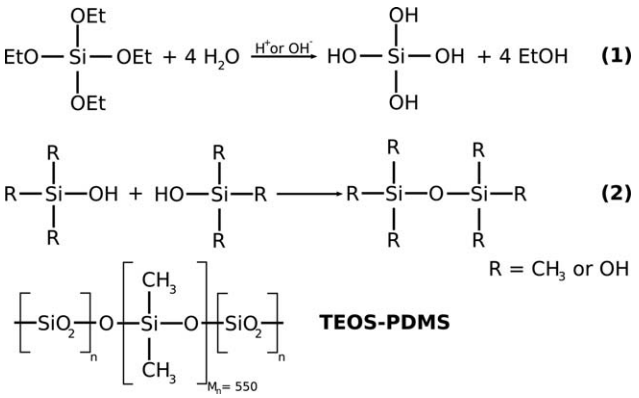

Figure 3. Reactions taking place in the formation of TEOS-PDMS. Reaction 1 is the acid- or base-catalyzed hydrolysis of the TEOS ethoxy groups into hydroxyl groups. Subsequently, in a polycondensation reaction the silanol groups of both PDMS and the hydrolyzed TEOS condense to form Si-O-Si bonds (reaction 2). In the TEOS-PDMS end product the condensed TEOS particles are depicted for simplicity as SiO_2.

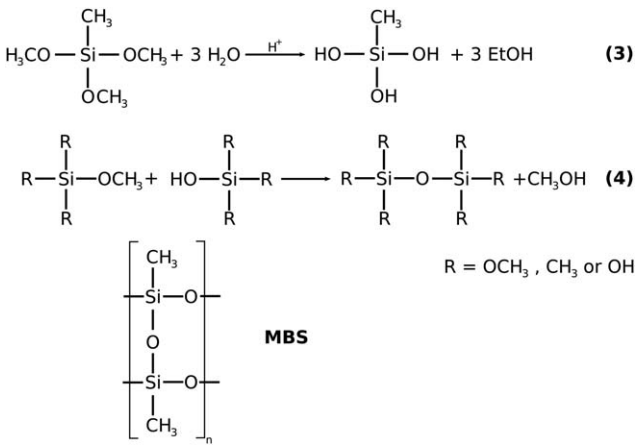

Figure 4. Reactions taking place in the formation of MBS. Reaction 3 is the hydrolysis of methoxy groups by water to form hydroxyl groups on the precursor molecules (as shown for MTMS). Subsequently, in a condensation reaction the hydroxyl groups can react with each other (reaction 2 in figure 3) or a hydroxyl group can react with an unhydrolyzed methoxy group (reaction 4) to form Si-O-Si bonds. The end product is MBS and is schematically shown for the case where only MTMS is used as precursor.

PDMS chains, and IPA of the water (which is added in the next step). To this mixture of precursors and solvents, either HCl or NH_4OH solutions of various concentrations were added. The amount of the NH_4OH or HCl solution added was chosen such that the ethoxy group to water ratio was 1:1.5, i.e., an excess of water. In Figure 3, an overview is shown of the reactions taking place for the synthesis of TEOS-PDMS as well as the final product: a hybrid material of small silica particles interconnected by PDMS chains. The mixture was stirred for 1–5 hours at room temperature, while the beaker was covered with aluminum foil to minimize evaporation of the solvents. After stirring, the liquid was placed in a vacuum desiccator to evaporate part of the solvents and was subsequently cast in polystyrene petri-dishes. After drying the films were removed from the petri-dishes and the up to 2 mm thick outer rim of the samples formed by the meniscus was cut away to obtain free-standing films with a thickness in the range of 200–300 μm.

During the sol–gel formation of TEOS-PDMS films, both acidic (HCl) and basic conditions (NH_4OH) were evaluated (see reaction 1 in Figure 3). It was observed that under basic conditions, on the timescales used for the experiments, no polymerization took place. Possibly the pH was not high enough to efficiently catalyze the hydrolysis reaction of the ethoxysilane to the corresponding silanol, or the hydrolysis of the formed siloxanes bonds to the corresponding silanol becomes significant enough to inhibit complete condensation. On the other hand, acid catalyzed hydrolysis proved very efficient in obtaining solid films. The use of various amounts of hydrochloric acid concentrations did not noticeably affect the end product. Therefore, in this work, a 3.3 *M* hydrochloric acid solution was used to synthesize all coatings for further testing.

After sol–gel formation, a condensation reaction (2 in Figure 3) of hydrolyzed TEOS with either itself, or with the hydroxyl terminated PDMS results in the TEOS-PDMS final product. The gelation and curing of the resulting gels was done in a controlled, slow manner to avoid cracking of the films, which was observed upon rapid curing in open air. Crack-free films were obtained by placing the petri-dishes in a closed chamber with an IPA and THF saturated vapor phase, as obtained by also enclosing a beaker filled with an IPA/THF mixture. To tune the flexibility, coatings with a TEOS:PDMS ratio ranging from 2:1 to 1:2 were produced. Even after drying most of the films still were somewhat sticky, greasy, and soft, especially if a high PDMS content was used. On the other hand, the layers could easily be lifted from the substrate on which they were casted, so freestanding films were obtained for the transparency analysis. In fact, due to the large volume contraction upon solvent evaporation, the adhesion to any substrate appeared so poor that an additional adhering medium will be required if the TEOS-PDMS films are applied as a flexible protection layer on thin-film solar cells.

MBS Films

The main precursor for the synthesis of the MBS films was methyltrimethoxysilane (MTMS), to which one of the other precursors tetramethylorthosilicate (TMOS), dimethyl-dimethoxysilane (DMDMS), or phenyltrimethoxysilane (PhTMS) was added, depending on the desired material properties. In this study, a typical synthesis uses at least 75% MTMS precursor. For the synthesis, the mixture of precursors was heated to 100 °C in a Teflon beaker using an oil bath. Subsequently, a HCl solution in water was added, the amount of this was chosen such that the water to methoxyl ratio is 0.5 to ensure that half of the methoxyl groups per silicon can hydrolyze. This mixture was covered by aluminum foil and stirred for 4–15 minutes until the viscosity starts to increase. An overview of the reactions taking place and the end product are depicted in Figure 4. Again, a hydrolysis reaction (3) takes place first, followed by the condensation reaction (4) of the hydrolyzed precursor with either another hydrolyzed silane or with a methoxyl group of an unhydrolyzed silane. After stirring, the solution was placed in a vacuum desiccator for 1 minute to evaporate most of the methanol (which forms during synthesis) and water. Subsequently, the solution was cast into a petri-dish

(with vents) and placed in an ambient environment. This resulted in films of typically 300 μm thickness, which after curing did not feel soft or sticky.

When HCl was used as the catalyst for the hydrolysis, MBS films were formed in a reproducible manner. Increasing the HCl concentration resulted in faster reaction times (i.e., the time it takes for the viscosity to increase noticeably), but no significant differences were found in the resulting films. All the coatings used for further study in this work were synthesized using a $10-2$ *M* HCl solution. In contrast to the synthesis of TEOS-PDMS films, no organic solvent was required for the synthesis of MBS films. The methanol formed during the hydrolysis step of the MBS precursors acts as a solvent, eliminating the need to add additional solvents. Vigorous stirring and elevated temperatures were used to mix the water and precursors (at least partly) to start the hydrolysis reaction. Because of the more reactive nature of the methoxy moieties, compared to the TEOS-PDMS reaction, condensation was quite efficient, resulting in a cured product with less reactive groups, which in turn resulted in more firm films that are not sticky. The higher reactivity of this precursor is a result of the ability of a silanol to react with methoxy silanes as well as other silanols. This in contrast to the ethoxysilanes, which are not able to condense with silanols. An advantage of this reaction is that it allows further crosslinking of the material even when the viscosity rises, since an unreacted hydroxyl group does not necessarily require another hydroxyl group to be close, a methoxy group also works. This mechanism is expected to reduce the amount of reactive groups present in the extendedly cured material.

The exact stirring time required was found to be dependent on the composition and the amounts of precursors added. In general, it was observed that reactions involving MTMS + TMOS go faster than those with MTMS + DMDMS. This can be attributed to the higher reactivity of the TMOS precursor (i.e., a higher number of methoxy groups per silicon atom increases reactivity). In addition, for larger amounts of precursors (while using the same beaker) the evaporation of methanol proceeds more slowly, since the area to volume ratio is lowered, hence the viscosity increases slower. However, no noticeable differences in the final product were found when the synthesis takes longer. Since no additional solvents are added in this synthesis, the volume contraction due to solvent evaporation during drying is reduced to a minimum. Therefore, it was not necessary to apply a slow well-controlled drying procedure, so that this material can be handled a few hours after synthesizing it. In addition, casting onto various substrates can be done, although for the characterization described here we used only freestanding films.

Cerium Doping

Based on the ease of reproducible synthesis on a substrate described above and sufficient transmission as will be described further on, MBS was found to be the most promising candidate for further evaluation. Therefore, the possibility to produce cerium doped MBS layers was investigated. The cerium precursors used for this purpose were $Ce(NO_3)_3 \cdot 6H_2O$ and $CeCl_3 \cdot 7H_2O$ as Ce(III) source, and $Ce(NH_4)_2\ (NO_3)_6$ as Ce(IV) source. A concentration of 0.1 to 2 wt % of Ce precursors were mixed with the MBS precursors after which the beaker was placed in the oil bath. The cerium compounds as such did not dissolve in the MBS precursors, but did so when the HCl solution was added. Ce(IV) is an oxidizing agent, so directly after adding the HCl solution a violent reaction occurred for a few seconds. The synthesis with Ce(IV) was observed to proceed faster than those with Ce(III) precursors, which was comparable to the rate of the regular MBS synthesis, probably due to the stronger Lewis acid character of the Ce(IV) species. In some cases the reaction resulted in opaque films (indicating particle formation), this mainly happened when DMDMS was used as one of the MBS precursors or $CeCl_3 \cdot 7H_2O$ as cerium precursor. Therefore, all Ce-MBS coatings synthesized for further analyses were obtained using a 10:1 mixture of MTMS:TMOS and by only utilizing the $Ce(NO_3)_3 \cdot 6H_2O$ and $Ce(NH_4)_2\ (NO_3)_6$ precursors.

Characterization Techniques

After synthesis and a first inspection by the naked eye, films of the obtained polymer layers were first subjected to transmission measurements using a Varian Cary 5000 UV-Vis-NIR spectrophotometer. The spectrometer was used in a direct transmission configuration in which the sample was illuminated over an area of 2×8 mm^2. No refractive index matching medium was used during these measurements, so besides absorption in the film we should also account for reflections at the coating surfaces. This means that without any absorption in the films the transmission measured was approximately 93% (the refractive index of the films is about 1.43). Furthermore, all the results of the transmission analysis are presented together with the transmission of the CMX benchmark. This benchmark reference is the Ce doped CMX coverglass as typically applied in the present generation of rigid solar panels.

All samples evaluated in this study could easily be bended around a cylinder with a radius of 10 cm without signs of layer degradation such as cracking or permanent deformation. As this is already more than an order of magnitude better than required for the anticipated thin-film cell solar panel described in the introduction, the flexibility was not further elaborated in the present study. For other potential applications such as rolled-up blankets that put more stringent conditions on the flexibility of the layers, an additional in-depth analysis might be required.

For the density determination, the pycnometer method (Gay-Lussac 5 mL $\pm$ 0.001 mL) was used with an analytical balance (Mettler AE163 0–30 g $\pm$ 0.01 mg). Samples were measured in triplo accumulating to a standard deviation in the results of less than 3%.

Finally, only for the most promising material with respect to ease of production, as well as sufficient transparency, samples were produced that were subjected to outgassing tests at the facilities of the European Space Agency at ESTEC. A test procedure has been developed in which the coatings were subjected 24 hours to an elevated temperature of 125 °C in high vacuum (pressure $< 10^{-5}$ mbar). During this treatment a cold plate, which was kept at 25 °C, was located in the vicinity (approximately 15 mm) opposite to the samples in order to collect

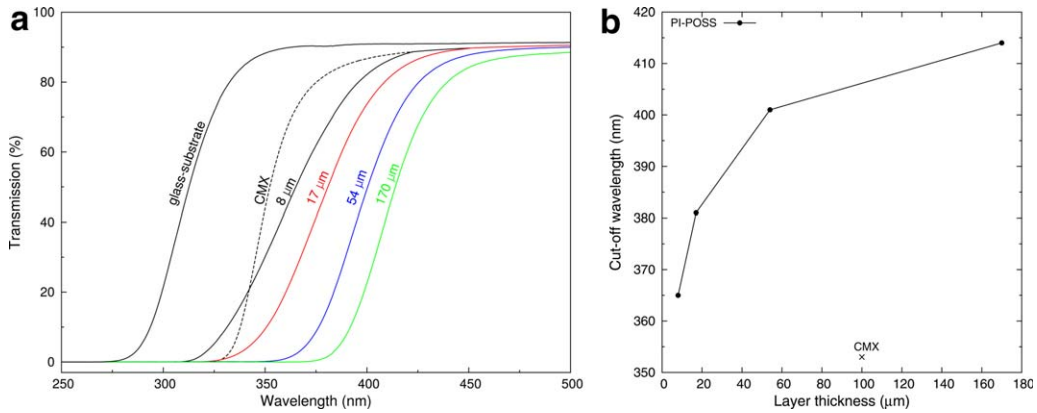

Figure 5. Transmission spectra of polyimide-POSS films of different thicknesses (as indicated at the curves) on glass substrates. For reference, the transmission of a 100 nm CMX coverglass, which is currently used for space solar panels, and the used glass substrate are also shown. [Color figure can be viewed in the online issue, which is available at wileyonlinelibrary.com.]

condensates. After the vacuum heat treatment, the films were allowed to recover for 24 hours under ambient conditions to re-establish the initial water film on the coating. The weight of the films was determined directly before and after the vacuum plus heat treatment and after recovery. From this, the Total Mass Loss (TML) and Recovered Mass Loss (RML) after testing and subsequent recovery were determined. In addition, the mass of the Collected Volatile Condensable Material (CVCM) at the cold plate is determined. Before and after the vacuum test the samples were stored in a humidity-controlled environment at 55% relative humidity. It should be noted that on earth everything in an ambient environment is covered with a thin layer of water, which evaporates while entering space. However, water is not harmful because it does not condense on any other part of the spacecraft, therefore in an outgassing test for space qualification one must be able to distinguish between the loss of water from the coatings and the loss of other products that potentially might be harmful. For space-qualified materials, RML has to be below 1% and CVCM has to be below 0.1%.[36]

RESULTS AND DISCUSSION

Transmission

Polyimide-POSS. In Figure 5(a), the transmission curves of polyimide-Polyhedral Oligomeric Silsesquioxan (PI-POSS) films of various thicknesses produced on glass substrates are shown, together with the transmission of the bare glass substrate and a CMX reference. In the wavelength range up to 450 nm, the transmission of the polyimide-POSS films is significantly less than the transmission of the CMX coverglass reference, especially as the layer thickness increases. Figure 5(b) shows the 50% transmission point for PI-POSS samples as a function of the layer thickness, indicating also their difference from the present applied CMX coverglass. This shows that that PI-POSS has a shifted 50% transmission relative to CMX making it less favorable for application as a transparent shielding layer. In a calculation based on the AM0 space solar spectrum and known quantum efficiency of the generally applied triple junction cells,[37] the potential loss in photocurrent by the application of the polyimide-POSS coatings was determined as compared to the CMX reference. These calculations indicate that depending on the thickness, the PI-POSS layers shown in Figure 5 will yield a reduced photocurrent of 1% up to 11% compared to the CMX reference. The fact that a layer of the required thickness loses > 10% of the photocurrent compared to CMX indicates that applying a polyimide-POSS layer, as flexible shielding coating will significantly reduce the performance of such cells, even if the material does not degrade at all in a space environment. Since one of the most transparent polyimides available was selected, the transmission analysis clearly indicates that polyimide-POSS coatings are not suitable as a flexible shielding layer for future space solar panels. Due to their low transparency, polyimide-POSS materials may only be useful for space applications if no light transmission through the material is required.

TEOS-PDMS. The TEOS-PDMS sol–gel synthesis resulted in films that ranged from fully transparent in the visible part of the spectrum, to white opaque films with a reduced transmission mainly at low wavelengths. In Figure 6, several

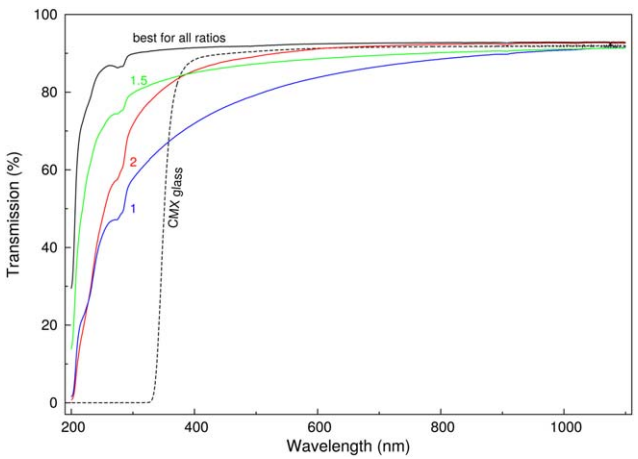

Figure 6. Transmission spectra of TEOS-PDMS films with a thickness of about 250 μm produced with TEOS/PDMS ratios of 1, 1.5 and 2. For each ratio the worst samples out of a batch of 5 are shown. The transmission curves for the best samples for each ratio are highly comparable and represented by the continuous black curve. For reference also the transmission curve of a CMX cover glass is shown. [Color figure can be viewed in the online issue, which is available at wileyonlinelibrary.com.]

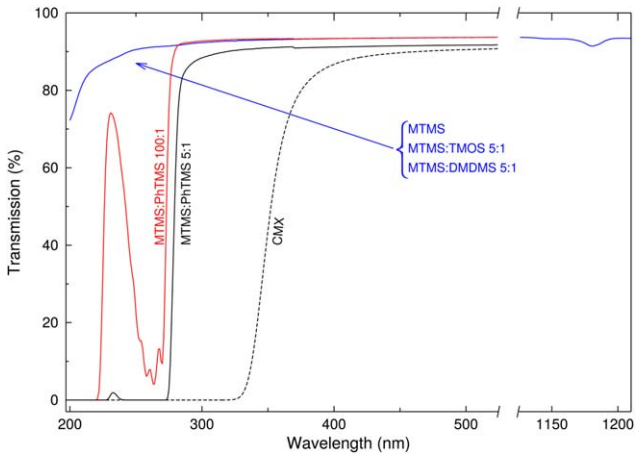

Figure 7. Transmission spectra of five MBS films of different composition and a CMX coverglass reference. [Color figure can be viewed in the online issue, which is available at wileyonlinelibrary.com.]

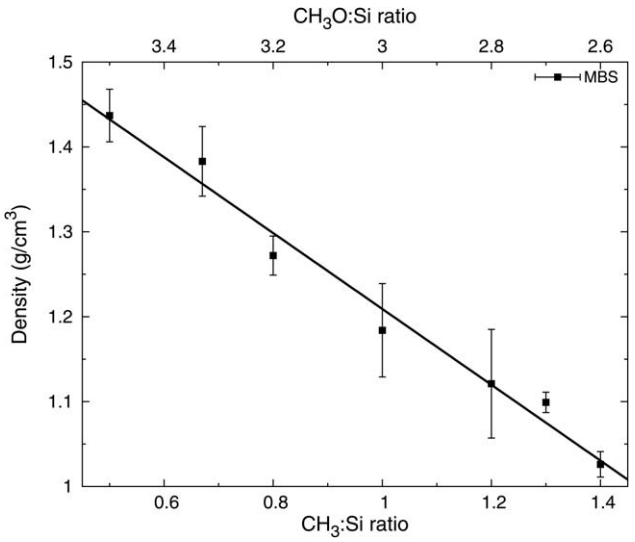

Figure 8. Density of MBS films as a function of the composition. CH_3:Si on the bottom axis and CH_3O:Si ratio on the top axis. A lower CH3:Si ratio means that on average a higher number of crosslinks can be formed per silicon atom. Adversely, the CH_3O:Si ratio indicates the amount of possible side groups per Si-atom. The line represents the best linear t through the data points which is averaged over a minimum of 5 samples.

transmission curves of free-standing TEOS-PDMS layers with a thickness of about 250 μm are shown. The coatings were produced with TEOS/PDMS ratios of 1, 1.5, and 2 in batches of five. Irrespective of the TEOS/PDMS ratio, the best films of each batch have a similar transmission characteristic as shown by the black curve in Figure 6. However, the transmission of the coatings within each batch varied considerably, as is shown by the worst sample of each batch in Figure 6. In some cases, the films were even completely opaque, so that no light was transmitted. The differences in transparency between films are attributed to the formation of small silica particles that reflect the light. This particle formation took place without any apparent relation to the parameters that were controlled during the synthesis, such as the composition of the material (i.e., the ratio of TEOS/PDMS), nor to the amount of solvent or HCl solution added. Based on the calculations using the AM0 solar spectrum and triple-junction cell quantum efficiency the potential photocurrent for the best TEOS-PDMS layers was found to be 4% higher than the CMX reference. For the worst samples out of each batch shown in Figure 6 the photocurrent ranges from a gain of 1% for the batch with TEOS/PDMS ratio 2 to a loss of 10% for the TEOS/PDMS ratio 1.

It could be concluded that, although the transmission analysis indicates a very good perspective for TEOS-PDMS films as flexible shielding layers for future space solar panels, in the current study we also encountered some major shortcomings from the production point of view. Because the solvents needed to avoid phase separation during TEOS-PDMS synthesis had to evaporate in a slow and controlled manner to avoid cracking of the films, the drying time required for the coatings was found to be quite long (up to a full week) and even then most coatings felt somewhat greasy. In addition, the large volume contraction makes it difficult to cast films of reproducible thickness and transparency. It also made it harder to cast adhering films on substrates, since the large volume contraction induces stress in the film, which frequently resulted in cracking or delamination.

MBS. To the naked eye, all synthesized MBS films appear highly transparent. This was confirmed by the transmission spectra of 300 μm thick MBS films as measured for different compositions (Figure 7). Clearly, the transmission of all MBS compositions is high over the relevant wavelength range, i.e., the near-infra-red, visible, and UV. The transmission spectra of the MTMS, MTMS:TMOS (5:1), and MTMS:DMDMS (5:1) films are virtually identical and therefore represented by a single curve in Figure 7. When the PhTMS precursor is used, the characteristic phenyl absorption band around 220–300 nm is observed. For higher phenyl contents (MTMS:PhTMS 5:1), this results in a total cut-off of the transmission for wavelengths below 275 nm. However, even for those films the transmission is still much better than that of CMX coverglasses, for which transmission already cuts-off around 350 nm. In the larger wavelength range up to 1250 nm, relevant for triple junction IMM solar cells, only a characteristic silicone absorption band of weak intensity around 1180 nm is found (see extension of Figure 7), otherwise the MBS material is fully transparent. Similar silicone absorption bands were observed in the adhesives currently used for mounting the CMX coverglasses and should therefore be no problem for use of MBS on top of a solar cell.

No opaque films were formed, even when the synthesis conditions were varied, this means there is a large process window to tune the material's properties in order to comply with the demands for a flexible shielding layer. Indeed, it was found that properties like the flexibility can be tuned by adding various amounts of TMOS, DMDMS, or PhTMS to the base precursor MTMS. Adding TMOS yielded more silica like material (making it more rigid, by reducing the amount of methyl groups), while adding DMDMS yielded more PDMS like material (increasing the flexibility). Using PhTMS resulted in phenyl groups being incorporated, which is not necessarily beneficial for the stability of the material in the environment encountered in space, but is

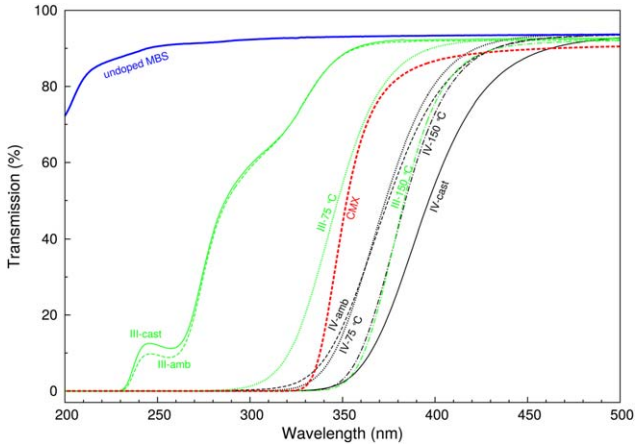

Figure 9. Transmission spectra of two MBS films with 1% Ce(III) (blue lines) or Ce(IV) (black lines) incorporated, for different curing times and methods. Both films have a thickness of approximately 250 μm. Indications stand for directly after casting (cast), after being stored for one week in an ambient environment (amb), cured for 16 hours at 75 °C (indicated) in a nitrogen environment, cured for 4 hours at 150 °C (indicated) in vacuum. Additionally shown an undoped MBS film. [Color figure can be viewed in the online issue, which is available at wileyonlinelibrary.com.]

expected to be advantageous for the flexibility, especially at low temperatures.[38]

Further Analyses of MBS Films

Given the ease of synthesis, high transparency, and reproducibility in obtained material quality, MBS layers are a very promising candidate to be applied as flexible shielding cover on future space solar panels. To determine the performance in relation to the CMX glass benchmark, the required thickness of the MBS layers, possibility for Ce doping, and vacuum stability of this material were evaluated in more detail.

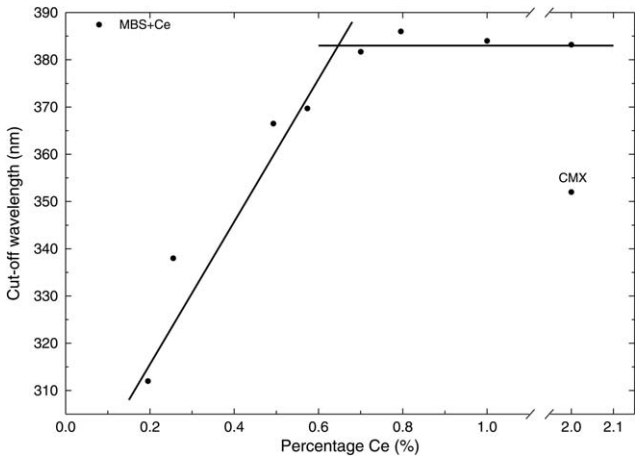

Figure 10. The 50% transmission points as a function of the cerium percentage in the extendedly cured (1 week ambient + 16 hours at 75 °C + 8 hours at 150 °C) Ce-MBS films, also shown is 50% transmission for CMX glass. The thickness of the Ce-MBS films is approximately 250 μm and that of CMX glass is 100 m. The lines serve to guide the eye. [Color figure can be viewed in the online issue, which is available at wileyonlinelibrary.com.]

Table I. Total Mass Loss (TML), Recovered Mass Loss (RML), and Collected Volatile Condensable Material (CVCM) After Outgassing Tests of MTMS:DMDMS (1:1) Coatings Cured for Various Durations at Different Temperatures under Vacuum

Curing conditions	TML (%)	RML (%)	CVCM (%)
16 h 75 °C	3.29	0.10	0.06
16 h 75 °C 1h vac 150 °C	1.47	1.38	0.03
16 h 75 °C 1h vac 150 °C	0.31	0.22	0

Density. Material density analysis (Figure 8) shows that the density of MBS films is significantly lower than that of CMX glass, which has a density of 2.6 g/cm^3, but can be tuned by varying the materials composition. The CH_3:Si ratio in Figure 8 is the average number of CH_3 groups per silicon atom in the precursor mix used to synthesize the layers. This ratio is 1 for a 100% MTMS film (and those with PhTMS), and will go down if TMOS (CH_3:Si = 0) is added or up if DMDMS (CH_3:Si = 2) is used. A lower ratio also means that a higher number of cross-links can be formed, this explains the increasing density with the lowering of the CH_3: Si ratio in the used precursor mix. Gutina *et al.*[39] suggested that the CH_3: Si ratio has to be equal to or larger than 1 to obtain crack-free films. However, by applying a methanol saturated vapor surrounding during drying for samples produced with more than 25% TMOS (CH_3:Si = 0.75) we managed to synthesize 300 μm thick crack-free films from a precursor mixture with a CH_3: Si ratio of 0.5.

Ce Doping. During the reaction in the HCl solution and directly after casting, it was noticed that MBS with Ce(IV) was yellow-red (but transparent) in color while the Ce(III) films were nearly colorless. During subsequent room temperature curing the color of Ce-MBS changed to light brown, independent of the type of Ce precursor used. The tested Ce-MBS films were all transparent and showed a slight brown color, especially if a cerium content of more than 0.5% was used. In Figure 9, the transmission spectra of two MBS films are shown, one synthesized with a 1% Ce(III) and one with a 1% Ce(IV) precursor. It is known from literature[40] that the oxidation state of cerium can change during synthesis and subsequent curing. Therefore, the transmission of these two Ce-MBS films was measured a

Table II. Total Mass Loss (TML), Recovered Mass Loss (RML) and Collected Volatile Condensable Material (CVCM) After Outgassing Tests for Coatings of Different Compositions as Identified by the CH_3O:Si Ratio of the Initial Mixture

Composition	CH_3O:Si	TML (%)	RML (%)	CVCM (%)
MTMS:TMOS (4:1)	3.2	1.95	0.22	0
MTMS:TMOS (10:1)	3.1	1.00	0.31	0
MTMS	3	0.26	0.12	0
MTMS:DMDMS (10:1)	2.9	0.2	0.12	0
MTMS:DMDMS (4:1)	2.5	0.30	0.19	0.01

Before testing the films were cured for 16 h at 75°C and subsequently for 8 h at 150°C.

Table III. Overview of the Design/Selection Criteria and Positive or Negative Performance of Evaluated Materials on Each

Criteria	Materials		
	PI-POSS	TEOS-PDMS	MBS
Synthesis: Coating of aimed thickness	−	−	+
Reproducibility in material quality	+/−	−	+
Flexibility (bending radius < 10 cm)	++	++	++
Transparency (equal/better than CMX)	−	++	+
Ability for Ce-doping (up to 2% cf. CMX)			+/−
Vacuum stability (CVCM < 0.1%)			+

The possibility for Ce-doping and vacuum stability were only evaluated for MBS.

few hours after casting i.e., as soon as the coatings where not sticky anymore and could be handled with ease, and after a number of subsequent curing steps taking place at increasingly higher temperatures. These curing steps are: (1) a week under ambient conditions, (2) 16 hours at 75 °C in a nitrogen environment, and (3) 4 hours at 150 °C in vacuum, respectively. After passing the last step, the films will be referred to as extendedly cured.

Figure 9 shows that there is a significant difference in transmission between the films. Directly after casting and after a week of curing under ambient (amb) conditions, the Ce(III) film clearly shows absorption due to the 4f → 5d transitions around 250 and 300 nm. Related to the strong charge transfer absorption the Ce(IV) doped coatings show a 50% transmission cut-off (wavelength for which the transmission is 50%) at significant larger wavelength (about 400 nm) than the Ce(III) and undoped films. After curing under ambient conditions, the transmission cut-off shifts to a lower wavelength of about 370 nm, presumably due to a change in the chemical surrounding of the cerium ion. After curing the films for 16 hours at 75 °C in a nitrogen environment the transmission cut-off of the Ce(IV) doped coatings does practically not change as compared to curing under ambient conditions, while the transmission cut-off of the Ce(III) doped coatings increases significantly to about 350 nm. Curing the films for 8 hours at 150 °C in vacuum resulted in virtually identical transmission spectra with a transmission cut-off at 380 nm. Apparently, during curing (part of) the Ce(III) oxidizes to form Ce(IV) oxides, so that due to the strong charge transfer absorption of Ce(IV) all high energy photons were absorbed. Figure 9 shows that the transmission of the extendedly cured Ce doped MBS layers is less than the CMX reference. Based on the earlier described calculations using the AM0 solar spectrum and triple-junction cell quantum efficiency it was calculated that this corresponds to a reduction of about 3% in the potential photocurrent which signifies the need to optimize the curing procedure.

Figure 10 shows the 50% transmission cut-off wavelength for MBS films as a function of their Ce concentration. When the concentration of cerium is lowered, the transmission cut-off initially remains more or less constant until at doping levels below 0.7% the cut-off shifts to lower wavelengths. The coatings used for this figure were all extendedly cured, i.e., subjected to all the previously mentioned curing steps and gave virtually identical results for both Ce-precursors. For the lowest concentrations of cerium, the Ce(III) absorption feature of the 4f → 5d transitions around 250 nm remained visible, even after curing. This indicates that only part of the cerium oxidizes to Ce(IV) and if a Ce(IV) precursor is used it partly converts to Ce(III). The exact percentage of cerium in CMX is not revealed by the vendor, but is expected to be at least 2%.[34] The relative low cut-off wavelength of the CMX coating is related to the fact that it is 2.5 times thinner than the MBS coatings and possibly also to differences in chemical surrounding of the cerium compounds. No change in flexibility was observed in MBS films as a result of the incorporation of cerium.

Vacuum Stability. Primarily based on the ease of syntheses and application, in combination with sufficient transparency and proven suitability for Ce doping, MBS was selected to further study its potential to be applied as a flexible shielding layer for solar cells in space applications. Therefore, three batches of MBS films (without Ce doping) were produced as described in the Experimental/MBS films section and subjected to the above described outgassing procedure in order to determine a curing method that yields space qualified films with respect to vacuum stability.

In Tables I and II, the results of the measurements are shown, the first showing a coating of MTMS:DMDMS (1:1) which was cured increasingly longer and at higher temperatures. Clearly, the coating shows a decreasing Total Mass Loss (TML) and Recovered Mass Loss (RML) upon intensified curing. When all the reactive groups of the precursors react, the mass of the resulting MBS film is 50% of the mass of the precursors, due to the formation of methanol (and some water). The 0.1% mass loss in the outgassing experiments is therefore most likely due to evaporation of methanol that is still present in the film after curing at 75 °C. Table II shows different compositions of materials ordered according to the methoxyl-to-silicon ratio of the used precursor mix (first column). The methoxyl-to-silicon ratio indicates the reactivity of the starting materials: the higher the ratio the more reactive the precursor. A methoxyl-to-silicon ratio above 2 means the precursor mixture has possibilities to form side-chains (crosslinks) and is

expected to form these increasingly with increasing ratio. However, since the formation of crosslinks also depends on the diffusion of forming chains in the reaction mixture and curing product, not all methoxyl groups might have reacted during synthesis and curing. Therefore, it is possible that some remaining methoxyl groups evaporate during outgassing tests, since they are more easily evaporated than for example the more covalent bonded methyl groups. However, since they refrain from condensing it is considered unimportant and we focus on Collected Volatile Condensable Material (CVCM) as the most important parameter in this study.

The CVCM was below 0.1% for all coatings shown in Tables I and II. In fact, the CVCM was zero for all but three samples. These particular films contained a high percentage of DMDMS, which is the least reactive precursor (containing only two methoxyl groups) and is one that does not form crosslinks. Therefore, the CVCM detected is likely to be either unreacted DMDMS, or short linear chains that can evaporate in vacuum. When more intense curing is performed, however, even these films show a CVCM of near 0%. Since the CVCM is zero for most samples, the RML should almost fully be attributed to the evaporation of methanol and water formed during synthesis, since these, just as ambient water, do not condense on the cold plate. This is further confirmed by the fact that the coatings produced with TMOS show a significantly higher level of TML compared to the other coatings.

The outgassing tests show that curing the films in vacuum at elevated temperatures for 8 hours, will evaporate most of the volatile reaction products beforehand. It also shows that the evaporated molecules are unlikely to condense on nearby surfaces of a satellite (i.e., CVCM is zero), meaning that the evaporation of solvents in space should not be a problem. For the outgassing tests, the films were cut into small pieces, so no flexibility measurements could be performed afterwards. Therefore, MBS coatings were also kept under high vacuum and at elevated temperatures to simulate the conditions during the outgassing tests at ESTEC. After the vacuum treatment the flexibility of the films had not changed, indicating that evaporation of the solvents in the samples has no noticeable effect on the flexibility of the films.

These measurements indicate that, in this phase of development, MBS is suited for further space qualification testing at ESA-ESTEC without the risk of contaminating the required dedicated equipment. In fact, part of these tests involving irradiation hardness and UV stability tests have already been performed and the results are reported elsewhere.[41] The current study indicates that further research on MBS should also include tuning of the Ce doping level in relation to the circumstances encountered for each particular mission in order to optimize output of the photovoltaic-system.

CONCLUSIONS

In this study, three candidate materials that potentially can be applied as a transparent shielding layer for the next generation of flexible space solar panels have been identified and studied for their suitability. The results of the study are summarized in Table III. As there are no clear design criteria for synthesis, the preference in this respect is based on the mutual comparison of the different materials.

For PI-POSS, the necessity to apply multi-step casting to produce coatings of sufficient thickness and also the variation in transmission cut-off wavelength with the thickness of the layer is a clear disadvantage. Furthermore, the material was found unsuited because for a coating of the required thickness, the transmission loss in the wavelength range covered by the generally applied triple junction space solar cells was calculated to result in a photocurrent loss of >10% compared to the currently applied CMX coverglasses.

For a wide range of compositions, the best TEOS-PDMS based films are highly transparent in the investigated 200–1250 nm wavelength range (significantly better than CMX glass). However, the solvents required to avoid phase separation during synthesis of the materials give rise to a large volume contraction, which made it virtually impossible to cast adhering films of reproducible thickness and quality on any type of substrate. Without any obvious reason samples produced directly after each other from the same batch and same process conditions also showed significant variation in transparency ranging from highly transparent to translucent and even fully opaque white films (probably due to the formation of small silica particles). TEOS-PDMS might therefore be, in theory, well suitable as a flexible transparent shielding layer for space solar panels, if the synthesis can be better controlled than in the present study.

However, casting of MBS films of reproducible thickness and transparency was found to be relatively easy. The coatings are almost fully transparent in the investigated 200 to 1250 nm wavelength range. Therefore, this material was selected for further investigations in which it was demonstrated that cerium (used in currently applied CMX glass to increase radiation hardness) can be effectively incorporated during MBS synthesis. Transmission measurements of the extendedly cured Ce doped MBS layers show a reduced transparency compared to the CMX reference, which was calculated to correspond to a reduction of about 3% in the potential photocurrent. This potential drawback (indicated with +/– in Table III) signifies the need to further optimize the curing procedure. Finally, all batches of cured MBS films have passed the vacuum stability tests, so that this material can be subjected to further space qualifications tests without the risk of contaminating the required dedicated equipment.

ACKNOWLEDGMENTS

This work was financially supported by the Netherlands Space Office (NSO) under project number PEP 61727 DS and by the ESA NPI program under the project number E/0900-05-01018. The authors would like to thank Stephen Taylor (ESTEC) and Steffen van der Wal (Utrecht University) for fruitful discussions. Furthermore, we would like to thank Paul Kouwer (Radboud University) for discussion and feedback.

REFERENCES

1. Schermer, J.; Mulder, P.; Bauhuis, G.; Larsen, P.; Oomen, G.; Bongers, E. *Prog. Photovoltaics Res. Appl.* **2005**, *13*, 587.
2. Tatavarti, R.; Wibowo, A.; Martin, G.; Tuminello, F.; Youtsey, C.; Hillier, G.; Pan, N.; Wanlass, M.; Romero, M. Photovoltaic Specialists Conference (PVSC), 35th IEEE, **2010**, pp 002125–002128.
3. Yoon, J.; Jo, S.; Chun, I. S.; Jung, I.; Kim, H. S.; Meitl, M.; Menard, E.; Li, X.; Coleman, J. J.; Paik, U. *Nature* **2010**, *465*, 329.
4. Konagai, M.; Sugimoto, M.; Takahashi, K. *J. Cryst. Growth* **1978**, *45*, 277.
5. Yablonovitch, E.; Gmitter, T.; Harbison, J.; Bhat, R. *Appl. Phys. Lett.* **1987**, *51*, 2222.
6. Voncken, M.; Schermer, J.; Van Niftrik, A.; Bauhuis, G.; Mulder, P.; Larsen, P.; Peters, T.; deBruin, B.; Klaassen, A.; Kelly, J. *J. Electrochem. Soc.* **2004**, *151*, G347. G352.
7. Voncken, M.; Schermer, J.; Bauhuis, G.; Mulder, P.; Larsen, P. *Appl. Phys. A* **2004**, *79*, 1807.
8. Bissels, G.; Asselbergs, M.; Bauhuis, G.; Mulder, P.; Haverkamp, E.; Vlieg, E.; Schermer, J. *Sol. Energy Mater. Sol. Cells* **2012**, *104*, 97.
9. Bauhuis, G.; Mulder, P.; Haverkamp, E.; Schermer, J.; Bongers, E.; Oomen, G.; Kostler, W.; Strobl, G. *Prog. Photovoltaics Res. Appl.* **2010**, *18*, 155.
10. Bauhuis, G.; Mulder, P.; Haverkamp, E.; Huijben, J.; Schermer, J. *Sol. Energy Mater. Sol. Cells* **2009**, *93*, 1488.
11. Schermer, J.; Mulder, P.; Bauhuis, G.; Voncken, M.; Van Deelen, J.; Haverkamp, E.; Larsen, P. *Phys. Status Solidi A* **2005**, *202*, 501.
12. Schermer, J.; Bauhuis, G.; Mulder, P.; Haverkamp, E.; Van Deelen, J.; Van Niftrik, A.; Larsen, P. *Thin Solid Films* **2006**, *511*, 645.
13. Green, M. A.; Emery, K.; Hishikawa, Y.; Warta, W.; Dunlop, E. D. *Prog. Photovoltaics Res. Appl.* **2012**, *20*, 606.
14. Kayes, B. M.; Nie, H.; Twist, R.; Spruytte, S. G.; Reinhardt, F.; Kizilyalli, I. C.; Higashi, G. S. In Photovoltaic Specialists Conference (PVSC), 37th IEEE, **2011**, pp 000004–000008.
15. Miller, O. D.; Yablonovitch, E.; Kurtz, S. R. *IEEE J. Photovoltaics* **2012**, *2*, 303.
16. Geisz, J.; Kurtz, S.; Wanlass, M.; Ward, J.; Duda, A.; Friedman, D.; Olson, J.; McMahon, W.; Moriarty, T.; Kiehl, J. *Appl. Phys. Lett.* **2007**, *91*, 3502.
17. McGrath, B.; Schönbacher, H.; Van deVoorde, M. *Nucl. Instrum. Methods* **1976**, *135*, 93.
18. Treadaway, M. J.; Passenheim, B. C.; Kitterer, B. D. *IEEE Trans. Nucl. Sci.* **1975**, *22*, 2253.
19. Kitchen, C.; Mullaney, K.; Price, M.; Dollery, A.; Fyles, K.; Eaves, H.; Crabb, R.; Bula, P. Sep, In Photovoltaic Specialists Conference, **1997**, Conference Record of the 26th IEEE, pp 1011–1014.
20. Levy, P. W. *Proc. SPIE 0541: Radiat. Effects Opt. Mater.* **1985**, *2*,
21. Clough, R. L.; Billingham, N. C.; Gillen, K. T.; Adams, M. R.; Polymer Durability–Degradation, Stabilization, and Lifetime Prediction, Amer. Chemical Soc., **1996**, Vol. *249*.
22. Haruvy, Y. *ESA J.* **1990**, *14*, 109.
23. Kiefer, R. L.; Herring, K.; Wylie, B. J.; Orwoll, R. A.; Thibeault, S. A. *Polym. Int.* **1999**, *48*, 1042.
24. Young, P. R.; Slemp, W. S. *Polym. Adv. Technol.* **1998**, *9*, 20.
25. Duo, S.; Li, M.; Zhu, M.; Zhou, Y. *Mater. Chem. Phys.* **2008**, *112*, 1093.
26. Verker, R.; Grossman, E.; Eliaz, N. *Acta Mater.* **2009**, *57*, 1112.
27. Pielichowski, K.; Njuguna, J.; Janowski, B.; Pielichowski, J. Supramolecular Polymers Polymeric Betains Oligomers, Springer, **2006**, pp 225–296.
28. Phillips, S. H.; Haddad, T. S.; Tomczak, S. J. *Curr. Opin. Solid State Mater. Sci.* **2004**, *8*, 21.
29. Dever, J. A.; Banks, B. A.; Yan, L. *J. Spacecraft Rockets* **2006**, *43*, 386.
30. Zimmermann, C. G. *J. Appl. Phys.* **2008**, *103*, 083547.
31. Widmaier, J. M.; Bonilla, G. *Polym. Adv. Technol.* **2006**, *17*, 634.
32. Mackenzie, J. D.; Chung, Y.; Hu, Y. *J. Non-Cryst. Solids* **1992**, *147*, 271.
33. Haruvy, Y.; Webber, S. *Chem. Mater.* **1991**, *3*, 501.
34. Gvishi, R.; Strum, G.; Shitrit, N.; Dror, R. *Opt. Mater.* **2008**, *30*, 1755.
35. Huang, H. H.; Orler, B.; Wilkes, G. L. *Macromolecules* **1987**, *20*, 1322.
36. ESTEC European Cooperation for Space Standardization: Esa Requirements and Standards Division; ecss-q-st-70-02c, **2008**.
37. Sato, S.; Ohshima, T.; Imaizumi, M. *J. Appl. Phys.* **2009**, *105*, 044504.
38. Zimmermann, C.; Pueyo, D.; Semprimoschnig, C.; Taylor, S. Photovoltaic Specialists Conference, PVSC '08, 33rd IEEE, **2008**, pp 1–4.
39. Gutina, A.; Haruvy, Y.; Gilath, I.; Axelrod, E.; Kozlovich, N.; Feldman, Y. *J. Phys. Chem. B* **1999**, *103*, 5454.
40. Pepe, A.; Aparicio, M.; Ceŕe, S.; Duŕan, A. *J. Non-Cryst. Solids* **2004**, *348*, 162.
41. Smeenk, N.; Mooney, C.; Feenstra, J.; Mulder, P.; Rohr, T.; Semprimoschnig, C.; Vlieg, E.; Schermer, J. *Polym. Degrad. Stabil.* **2013**, *98*, 2503.